

Wavelength considerations in confocal microscopy of botanical specimens

by M. D. FRICKER* and N. S. WHITE†, **Department of Plant Sciences, University of Oxford, South Parks Road, Oxford OX1 3RB*
and †*Department of Zoology, University of Oxford, South Parks Road, Oxford OX1 3PS, U.K.*

KEY WORDS. Multiple-wavelength confocal microscopy, ultraviolet, chromatic aberration, confocal ratio imaging, HeCd laser, chromosomes, guard cells.

SUMMARY

We have used a multiple-laser confocal microscope with lines at 325, 442, 488, 514 and 633 nm to investigate optical sectioning of botanical specimens over a wide range of wavelengths. The 442-nm line allowed efficient excitation of Chromomycin A3, with minimal background autofluorescence, to visualize GC-rich heterochromatin as an aid to chromosome identification. Sequential excitation with 442- and 488-nm light enabled ratio imaging of cytosolic pH using BCECF. The red HeNe laser penetrated deep into intact plant tissues, being less prone to scattering than shorter blue lines, and was also used to image fluorescent samples in reflection, prior to fluorescence measurements, to reduce photobleaching. Chromatic corrections are more important in confocal microscope optics than in conventional microscopy. Measured focus differences between blue, green and red wavelengths, for commonly used objectives, were up to half the optical section thickness for both our multi-laser system and a multi-line single-laser instrument. This limited high-resolution sectioning at visible wavelengths caused a loss in signal. For ultraviolet excitation the focus shift was much larger and had to be corrected by pre-focusing the illumination. With this system we have imaged DAPI-stained nuclei, callose in pollen tubes using Aniline Blue and the calcium probe Indo-1.

INTRODUCTION

Application of confocal microscopy to botanical specimens

Light microscopy has been extensively used for structural and histochemical studies of fixed plant material and to probe dynamic processes in living cells (Robards, 1985). Fluorescence microscopy gives high contrast for localization of specific subcellular structures such as the cytoskeleton (Lloyd, 1987), and allows quantitative measurement of a growing number of metabolites and ions such as Ca^{2+} (Read *et al.*, 1992). Plant cells present specific problems that both invite and confound investigation by confocal microscopy. Physical exclusion of out-of-focus information at the confocal aperture is particularly advantageous with highly scattering and diffractive plant cells, especially sampling deep within intact tissues. Unfortunately, refraction by the cell wall also produces effects similar to spherical aberration, giving non-uniform optical sectioning.

Plant cells also contain many pigments with complex absorption, scattering and autofluorescence spectra which complicate wavelength-dependent imaging techniques. An example is chlorophyll which absorbs both red and blue light, fluorescing at wavelengths above 650 nm.

Confocal microscopy at different wavelengths

The confocal microscope requires highly collimated illumination to achieve its unique optical sectioning through rejection of out-of-focus light returning from the sample (Minsky, 1961; Shotton, 1989). The confocal tandem scanning microscope (TSM) uses a mercury or xenon arc lamp, with the advantage of several high-intensity lines suitable for reflection and absorption contrast (Petran & Hadravsky, 1967; Boyde, 1985). Confocal fluorescence images can be recorded using intensified or cooled charged coupled device (CCD) video cameras. Beam scanning microscopes exploit the inherent collimation of laser sources to provide diffraction-limited, point illumination at well-defined wavelengths. Commercial confocal scanning laser microscopes (CSLMs) first appeared with single inexpensive lasers, such as the red helium neon (HeNe), primarily for reflection contrast imaging. More recently, multiple laser systems have been developed for colour reflection imaging in materials science (Lasertech Corporation, Yokohama, Japan) and biological specimens (Cogswell & Sheppard, 1990). Fluorescence measurements using CSLMs have been driven primarily by the availability of stable, low-power, single-mode lasers at appropriate wavelengths. Argon-ion lasers have proved excellent for efficient excitation of fluorescein and its derivatives at 488 nm. Rhodamine-based dyes can also be excited with the 514- or 529-nm lines of argon-ion lasers, but more effectively with the green helium neon (e.g. the GreNeTM from Melles Griot) 546-nm line. The recently introduced argon/krypton mixed-gas laser has lines at 488, 567 and 649 nm and provides an excellent solution for double labelling with fluorescein and Texas-Red conjugates. Triple labelling offers much potential, as the use of red excited dyes, such as the DiSC_n series and CY5TM, become more widespread. Red lines are also useful for transmission phase or reflection imaging to survey a sample before switching to fluorescence, as most common fluorescent dyes absorb weakly above 600 nm and therefore undergo little photobleaching.

A wide range of biologically important fluorochromes routinely used in conventional microscopy require excitation with blue, violet or ultraviolet (UV) wavelengths. There have been only a few attempts to extend the range of wavelengths available in the short blue and violet part of the visible spectrum, primarily to increase the resolution of confocal microscopes (Brakenhoff *et al.*, 1980). Some dyes with blue/violet excitation maxima, such as Lucifer Yellow (430 nm) and Chromomycin A3 (456 nm), can be imaged with the 488-nm argon-ion line, but the inefficient excitation reduces the signal-to-noise ratio and is far from ideal in living systems when excitation intensity needs to be minimized. Further enhancements of resolution by UV confocal transmission microscopy at 325 nm (Brakenhoff *et al.*, 1979) have been discussed. Confocal fluorescence excited at 325 or 351 nm (Kuba *et al.*, 1991) and at 364 nm (Montag *et al.*, 1991) has been recently demonstrated, but commercial instruments have been slow to appear for several reasons. First, correction for chromatic aberration becomes more difficult as the spread of wavelengths increases. Second, excitation intensity begins to be affected by transmission losses with most conventional microscope objectives and transfer optics below about 380 nm, and quartz optics are required for wavelengths below 340 nm. Third, progress in development of convenient UV lasers is countered by the trend towards development of visible alternatives to UV-excited fluorochromes.

In addition to multiple labelling studies, fluorescent ratio imaging is becoming increasingly important for monitoring temporal and spatial dynamics of cytosolic ion

activities. Monitoring a shift in either the excitation or emission spectrum of the dye on binding to the ion of interest can be easily achieved by quantification of the fluorescence at two wavelengths, typically corresponding to the peaks for the free and bound form. The ratio between these values automatically corrects for localized variations in dye concentration, cell shape, dye bleaching or leakage. Combination of fluorescence ratio techniques with confocal microscopy represents the optimum solution for quantitative measurement of optical probes. A range of dyes are now available for key ions, such as Ca^{2+} and H^{+} , which demand precisely tailored wavelength combinations. We have examined two permutations for imaging Ca^{2+} using Indo-1 (325-nm excitation, 405- and 480-nm emission) and Fura-RedTM (Molecular Probes; 425–450- and 480–500-nm excitation, 660-nm emission). The latter excitation wavelengths are also ideally suited to imaging the pH dye BCECF, whose emission maximum (530 nm) is sufficiently well spaced from Fura-Red to permit simultaneous measurement of cytosolic Ca^{2+} and H^{+} activities. Dynamic changes in these ions have been implicated in signal transduction of physiological stimuli in several plant systems including stomatal guard cells (Gilroy *et al.*, 1991). We have previously investigated the three-dimensional (3-D) shape and volume of guard cell vacuoles using the confocal microscope (Fricker & White, 1990), and describe here the imaging of cytosolic Ca^{2+} , using Indo-1, and quantitative techniques for imaging H^{+} by fluorescence excitation ratioing of BCECF in the guard cell system.

Microscopy techniques covering a broad spectral range demand precise registration of each wavelength for consistent sampling and accurate quantification. Correction for chromatic aberration has traditionally been achieved through careful selection of objective lens elements to bring two or three selected wavelengths across the spectrum to the same focus. Intermediate wavelengths are brought to slightly different foci, above or below this plane, depending on the lens design. The difference in focal plane with achromatic and apochromatic lenses is barely noticeable in conventional imaging, as it falls well within the depth of field. In confocal systems the depth of field is significantly reduced and the consequences of aberration more apparent. Additional correction may be necessary to achieve optimal confocal performance at more than one wavelength, for example during fluorescence and particularly multiple labelling studies. The simplest solution is to introduce pre-focusing of the excitation beam to counteract axial chromatic aberration introduced by other optical elements. This has so far only been implemented for UV fluorescence (Kuba *et al.*, 1991), but is relatively straightforward for multiple-laser systems. Lasers with multiple lines have intrinsically good lateral registration of each wavelength, which facilitates alignment of the instrument, but the options for chromatic compensation are curtailed unless the beams are separated and corrected individually.

In this paper we present our findings on some general wavelength-dependent processes that must be considered in confocal imaging, particularly with botanical specimens. We have investigated the performance of our multiple-laser confocal system at different wavelengths and report on its application to imaging several key fluorescent probes including UV-fluorophors and dual excitation ratio dyes.

MATERIALS AND METHODS

A multiple-laser confocal microscope system

The multiple-laser system was based around a standard CSLM (Bio-Rad MRC 600) attached to an inverted (Nikon Diaphot) microscope. A schematic diagram of the system is shown in Fig. 1. The excitation path was modified to receive four lasers covering the following wavelengths: 633 nm (3.5 mW HeNe, Spektra Physics); 514 and 488 nm (25 mW argon-ion, Bio-Rad Microscience/ILT Ltd); 442 nm (11 mW HeCd) and 325 nm (30 mW UV-HeCd, Lambda Photometrics Ltd). The three visible lasers

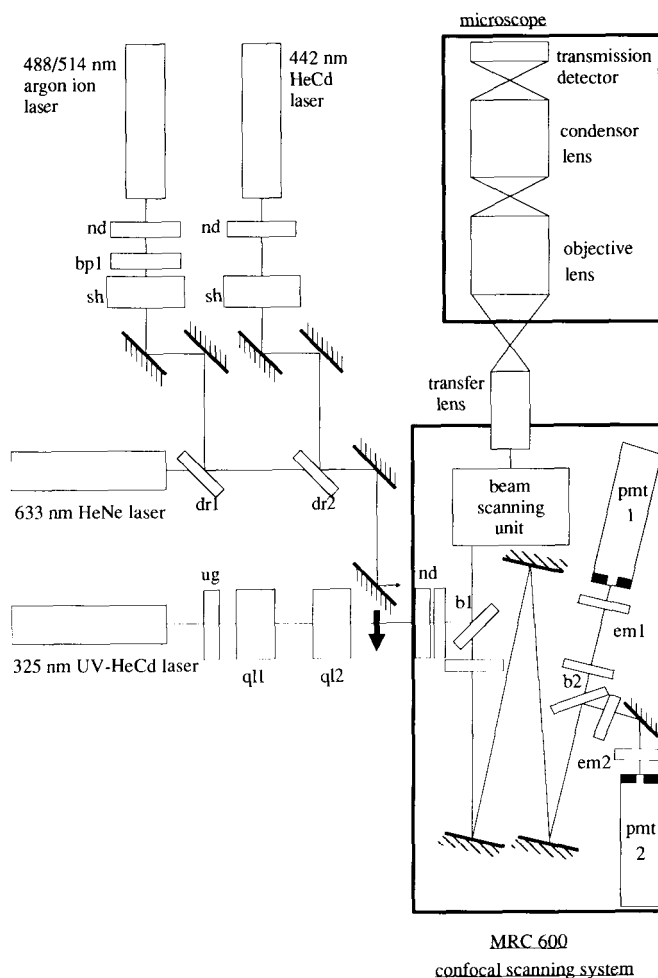


Fig. 1. A schematic diagram of the multiple-laser confocal microscope. Beam steering mirrors were used to co-align the four lasers onto a single optical axis into the confocal scanning system. Microscope: Nikon 'Diaphot' (inverted) or Zeiss 'Standard'. pmt1/pmt2 = MRC 600 channel 1 and 2 photomultipliers with variable confocal apertures. A sliding mirror (arrow) was used to switch rapidly between UV and visible illumination. nd = neutral density filter, bp1 = 488/514-nm band pass filter, sh = computer-controlled electronic shutter, dr1 = 580-nm dichroic reflector, dr2 = 455-nm dichroic reflector, ug = UG5 UV short-pass filter, ql1/2 = quartz, focusing beam expander, b1/2 = MRC 600 filter blocks, em1/2 = emission filters in front of pmt 1/2.

were combined via a series of dichroic mirrors and co-aligned on the same optical axis using beam steering mirrors. Electronic shutters ('Uniblitz', Vincent Associates, New York) were included for the argon-ion and blue HeCd lasers to enable rapid switching between excitation wavelengths during ratio measurements. Neutral density filters were used to balance the intensity of the two beams. The UV laser was introduced directly into the MRC 600 box to minimize attenuation by beam steering components. A focusing beam expander was used to both increase the beam diameter and pre-focus the UV beam to compensate for axial chromatic aberration in the microscope optics (see the section on *UV confocal fluorescence*). A sliding mirror was used to switch between UV and visible wavelengths. To increase the transmission of UV illumination, the transfer lens of the MRC 600 was replaced with a quartz $\times 8$ eyepiece (Bio-Rad

Microscience) and the Diaphot microscope substituted by an 'upright' system mounted horizontally on the optical table. This was a simple 160-mm tube length microscope stand (Zeiss 'Standard') with objective lens turret, focusing stage and substage condenser for transmission imaging. Fine focus control was by computer-driven stepper motor for both microscope stands.

Measurement of optical section width and axial position at visible wavelengths

To compare the sectioning performance of the confocal microscope system at wavelengths from 442 to 649 nm, vertical sections were collected in reflection contrast through a plane aluminium mirror. The spread or extent of the mean intensity, averaged over a central portion of the field and plotted against z distance, defined the overall sectioning characteristics (or plane z -response) at each wavelength. Axial chromatic aberration at each wavelength was estimated from the position of the maximum intensity in the plane z -response, relative to that of the 633-nm laser. To ensure accurate registration at different wavelengths in the multiple-laser Diaphot system, the red HeNe image was always collected into channel one as a reference, with the argon-ion or blue HeCd lasers collected simultaneously into channel two. Such dual-channel vertical sections were collected with different objective lenses, and transfer optics comprising the standard Nikon $\times 8$ eyepiece and $\times 1$ relay lens. To compare our multiple-laser system with a multi-line single-laser system, vertical sections were also collected on an MRC 600 system with an argon/krypton mixed gas laser and an upright Nikon Optiphot microscope with $\times 8$ eyepiece. Images at the common 488-nm line were used as reference points to compare these data with those from the multiple-laser Diaphot system.

Sample penetration and wavelength

The difference in sample penetration due to wavelength-dependent scattering was estimated from reflection contrast images of unstained, translucent root tissue. Serial optical sections were collected at 1- μ m intervals simultaneously at 633 nm (channel 1) and 442 nm (channel 2) through a primary root tip of 3-day-old *Cucumis sativus* seedlings at a region of vascular differentiation. The illumination and collection characteristics were approximately balanced for the two channels.

Fluorescence excitation efficiency

Chromomycin A3 banding patterns in chromosomes of *Scilla siberica* ($2n = 12$) were examined during pollen mitosis as an aid to chromosome identification (White *et al.*, 1991). Developing pollen grains from *S. siberica* were fixed in 45% acetic acid, followed by a 3:1 mixture of ethanol and acetic acid (30 min). Pollen grains were plated onto polylysine-coated cover slips, air dried and stained in Distamycin A (0.2 mg ml⁻¹) in McIlvaine's buffer supplemented with 5 mM MgCl₂, followed by Chromomycin A3 (CMA, 0.5 mg ml⁻¹, 30 min) in the same buffer. Slides were mounted in buffer comprising 50% of the anti-fading agent 'Citifluor' (Agar Scientific), 40% McIlvaine's buffer, 5 mM MgCl₂ and 10% glycerol. Images were displayed using the THRUVIEW™ (Bio-Rad Microscience Ltd) visualization program.

Ratio imaging

Epidermal strips from *Commelina communis* were mounted in an open perfusion system under CO₂-free conditions as described previously (Gilroy *et al.*, 1991). The perfusion medium comprised 50 mM KCl, 1 mM MES adjusted to pH 6.1 with KOH. Illumination between 400 and 420 nm was provided from the microscope transmission lamp via a variable interference filter. BCECF was loaded into the cytoplasm of selected guard cells by iontophoretic micro-injection to an estimated concentration of 50 μ M.

Stomatal apertures ranged from 6 to 12 μm at the start of each experiment. Cells were pre-focused initially in reflection contrast with the red 633-nm HeNe laser to minimize photobleaching. Confocal fluorescence optical sections were collected sequentially with the 442-nm HeCd and 488-nm argon-ion laser, with a $540 \pm 15\text{-nm}$ emission filter. After subtraction of a background signal measured in the centre of the stomatal pore, the ratio image was calculated pixel by pixel as the 488-nm image divided by the 442-nm image. Regions of low intensity in the 442-nm image corresponding to very low dye concentration were used as a mask to exclude these unreliable high variance values from the ratio image.

UV confocal fluorescence

The axial shift in focus between the 325-nm UV and visible wavelengths was much larger than the optical section thickness and most of the emission from the illuminated plane was removed by the imaging aperture as out-of-focus blur. A variable focusing system comprising a 20-mm bi-concave and 50-mm bi-convex pair of fused silica lenses was introduced into the UV-HeCd laser path to correct the illumination focus so that both excitation and detected emission were confocal in the specimen. Two methods were used to determine the best confocal position as the UV-HeCd laser could not be directly imaged in reflection mode. In the first method the visible HeCd was focused by the microscope objective onto the end of a polymer fibre bundle, to give a conventional (non-confocal) transmission signal detected from the other end of the fibre by one of the MRC 600 photomultiplier channels. The divergence of the UV laser was then adjusted using the focusing beam expander to give a sharp transmission autofluorescence image of the fibre tip without refocusing the objective. Since the polymer fibre bundle was directly coupled to the photomultiplier, no focus shift occurred between excitation and emission wavelengths. The second approach was to image a bright sample, such as Calcofluor-stained paper, in UV confocal fluorescence, and to adjust the beam divergence until maximum brightness and image contrast were obtained. In practice, approximate values could be pre-determined for particular objectives by the transmission method and small adjustments made while viewing a particular sample.

A range of UV fluorochromes and tissues were examined: nuclei were stained in intact epidermal strips of *Commelina communis* and root tips from *Allium cepa* with 0.1 μM DAPI. Three-dimensional serial sections were collected with excitation at 325 nm and emission between 400 and 520 nm. Indo-1 was loaded into selected guard cells by iontophoretic micro-injection as described for BCECF. Pollinated stigmas of *Cordia alliodora* were stained with 0.1% Aniline Blue in 50 mM potassium phosphate after being cleared in 8 N NaOH for 24 h and rinsed with distilled water.

RESULTS

Optical performance and wavelength

The width at half peak height of the reflection plane z -response was between 3.3 ± 0.2 and $5.8 \pm 0.2 \mu\text{m}$ using the $\times 10$ fluor 0.5-NA objective and between 0.50 ± 0.05 and $0.70 \pm 0.05 \mu\text{m}$ using the $\times 60$ plan-apo 1.4-NA oil-immersion objective for the six visible wavelengths examined (Fig. 2). The relative axial position of the peak varied according to objective lens and wavelength (Table 1). At 325 nm, the position of the peak illumination (and thus the reflection response) was more than 50 μm from the 442-nm maximum for the $\times 10$ fluor objective, before correction by the focusing optics.

Sample penetration and wavelength

Summation projections, each of thirty-two sections (1- μm intervals) from the 3-D reflection contrast images through the cucumber root at 633 and 442 nm, are shown in

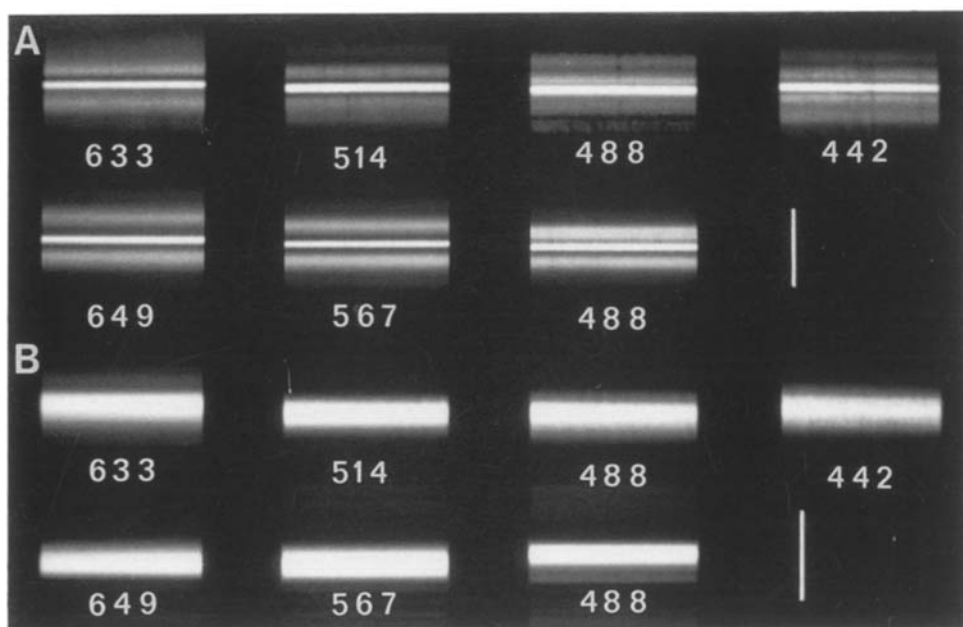


Fig. 2. Determination of the plane spread function at different wavelengths. A plane mirror was used as a test object and imaged in reflection mode using a Nikon fluor $\times 10$ 0.5-NA objective (A) or a Nikon plan-apo $\times 60$ 1.4-NA oil-immersion objective (B). A series of xz scans through focus at $0.4\text{-}\mu\text{m}$ ($\times 10$) and $0.1\text{-}\mu\text{m}$ ($\times 60$) intervals normal to the surface is presented in correct z -registration for the visible laser wavelengths indicated. Scale bar = $50\text{ }\mu\text{m}$ (A) and $2.5\text{ }\mu\text{m}$ (B).

Table 1. Relative axial position (μm) of the maximum intensity in the confocal reflection plane z -response for different objectives at particular wavelengths. Focus differences for all of the wavelengths considered were normalized and presented relative to the common 488-nm line of both microscope systems.

Configuration	Wavelength (nm)					
	442 (HeCd)	488 (argon) (Ar/Kr)	514 (argon)	567 (Ar/Kr)	633 (HeNe)	649 (Ar/Kr)
Multiple-laser Nikon Diaphot:						
$\times 10$ fluor 0.5-NA	-1.6 ± 0.2	0.0	-2.5 ± 0.2	—	-5.3 ± 0.2	—
$\times 60$ plan apo 1.4-NA	-0.10 ± 0.05	0.00	0.00 ± 0.05	—	-0.30 ± 0.05	—
Krypton/argon laser Nikon Optiphot:						
$\times 10$ fluor 0.5-NA	—	0.0	—	-2.0 ± 0.2	—	-5.8 ± 0.2
$\times 60$ plan apo 1.4-NA	—	0.00	—	$+0.30 \pm 0.05$	—	$+0.20 \pm 0.05$

Fig. 3. The projected regions were from $10\text{--}41\text{ }\mu\text{m}$ (A), $43\text{--}74\text{ }\mu\text{m}$ (B) and $76\text{--}108\text{ }\mu\text{m}$ (C). Strong signals were derived from cell walls orientated parallel to the surface. Initially, the intensities of bright features were comparable between the two wavelengths, but the signal from the blue laser faded more rapidly with increasing depth. There was correspondingly more contrast in the image from the blue laser due to greater scattering near the surface. At depth the red laser revealed more detail. Lignin thickening in xylem tissue was readily visible, even $100\text{ }\mu\text{m}$ deep into the tissue. However, some features (arrow in Fig. 3E) cannot be explained by this simple

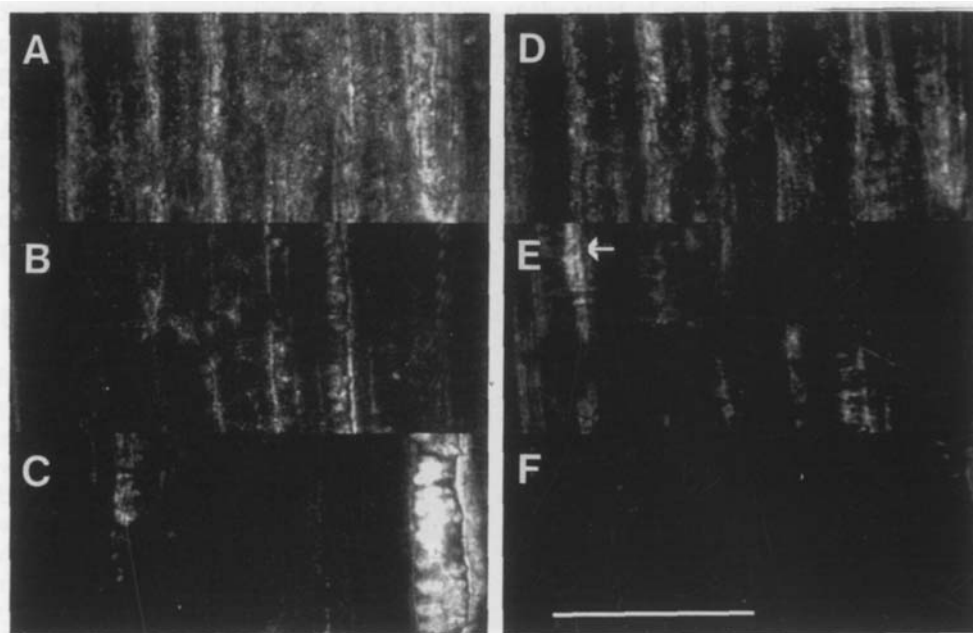


Fig. 3. Estimation of the depth of tissue penetration at different wavelengths. A region approximately 2 mm from the tip of an intact root from 3-day-old seedlings of *Cucumis sativis* was imaged in confocal reflection mode simultaneously at 633 nm (A–C) and 442 nm (D–F) to estimate the relative penetration achieved at different wavelengths in a botanical specimen replete with highly scattering cell walls. A total of 120 optical sections were collected at 1- μ m intervals using a Nikon fluor $\times 100$ 0.5-NA lens. Summation projections of thirty-two sections starting 10 μ m (A, D), 43 μ m (B, E) and 76 μ m (C, F) into the tissue are presented. Scale bar = 100 μ m.

scattering model. These probably arose from differential absorbance of the illumination and reflected light at the two wavelengths by some parts of the specimen.

Blue/violet excitation: Chromomycin A3 imaged at 442 nm

Chromomycin-A3-stained chromosomes were examined at all stages of the cell cycle during pollen mitosis in *Scilla siberica* ($2n=12$) with excitation at 442 nm. Intense bands of GC-rich heterochromatin were superimposed on the overall chromosome morphology which was indicated by a lower, general level of DNA staining (Fig. 4). The high-intensity chromomycin signal compared to autofluorescence enabled rapid chromosome identification using the THRUVIEW projection-based 3-D visualization methods (White *et al.*, 1991).

Dual-excitation ratio imaging: BCECF

Figure 5 illustrates dual-excitation ratio imaging of BCECF micro-injected into a single guard cell of a stomatal complex from *Commelina communis* with excitation at 442 and 488 nm. Fluorescence was visible in the peripheral cytoplasm and also in cytoplasmic strands traversing the vacuole. Within a single optical section (approximately 1 μ m thick) the signal was heterogeneous. The high signal throughout the nucleus for both wavelengths indicated the presence of a substantial concentration of dye within this organelle. The ratio image indicated that cytoplasmic pH remained relatively constant within the cytoplasm despite the variation in absolute intensity in different regions. The apparent lower pH in the nucleus was an artefact due to the saturation of the 488-nm signal necessary to bring out the cytoplasmic details.

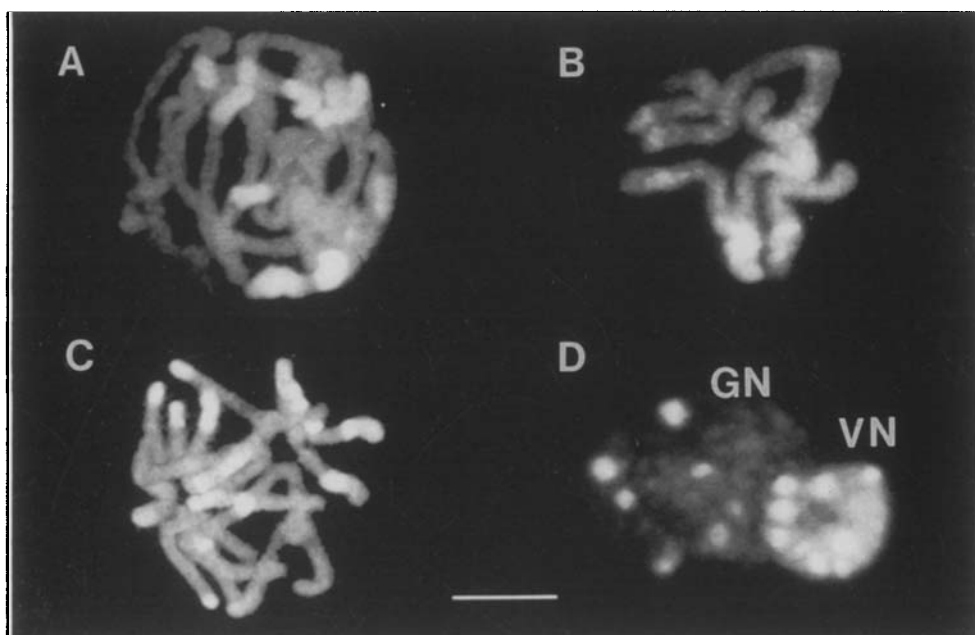


Fig. 4. Banding patterns of GC-rich heterochromatin in chromosomes of *Scilla siberica* during pollen mitosis revealed by staining with Chromomycin A3. Excitation at 442 nm, emission above 515 nm. Maximum projections of 15–30 optical sections collected at 0.5- μ m intervals using a Nikon plan-apo $\times 60$ 1.4-NA oil-immersion lens at prophase (A), metaphase (B), anaphase (C) and after formation of a bi-nucleate pollen grain (D). VN = vegetative nucleus, GN = generative nucleus. Scale bar = 5 μ m.

UV excitation: DAPI, Aniline Blue and Indo-1

DAPI-stained nuclei in intact epidermis (Fig. 6) were clearly visible with excitation at 325 nm. Autofluorescence from the wall provided a useful marker of cell shape. Image brightness drops off towards the edge of the field as a result of lateral chromatic aberration and field curvature restricting imaging to the centre of a reduced field using the MRC 'zoom' set to 2 or 3. Depth discrimination appears remarkably good in xz sections (Fig. 6C), residual aberrations being to some extent countered by the increased resolution of the shorter UV wavelengths. Individual chromosomes could be clearly distinguished during metaphase in *Allium* root tip cells (Fig. 7).

Selective staining of callose with Aniline Blue allowed easy visualization of compatible pollen tubes tens of micrometres into the stigma of *Cordia alliodora* (Fig. 8).

Preliminary results from UV imaging of the dual-emission Ca^{2+} dye, Indo-1, after micro-injection into guard cells, showed dye distributed through the cytoplasm and accumulated in the nucleus. There was no signal from the vacuole. A single optical section approximately 1.5 μ m thick cut tangentially near the base of the cell is shown in Fig. 9.

DISCUSSION

Optical performance and wavelength

Theoretical predictions for the z -response of an ideal confocal microscope are based on the illumination of the objective lens by a plane wave. Practical deviations from this arrangement include the Gaussian beam profile from most lasers. The measured plane z -responses from our system are consistent with this approximation. Predicted resolution increases at shorter wavelengths are masked by small variations in the beam divergence and profiles of the Gaussian argon-ion and HeNe lasers and those of the

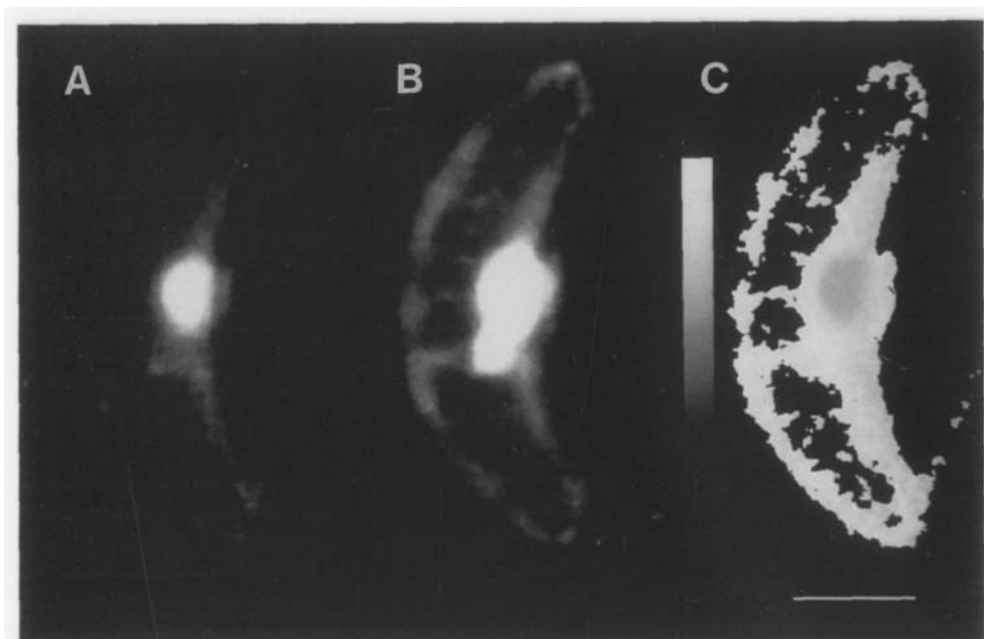


Fig. 5. Dual-excitation confocal ratio imaging of cytosolic pH in a single guard cell of *Commelina communis* loaded with BCECF by iontophoretic micro-injection. Single optical sections were collected near the mid-plane of the cell using a Nikon fluor $\times 40$ 0.85-NA lens. Sequential excitation at a pH-independent wavelength (442 nm, A) and a pH-dependent wavelength (488 nm, B) was achieved by electronic shuttering of the argon and visible HeCd lasers. The emission signal from BCECF was separated from chloroplast autofluorescence using a 515-nm dichroic and 540 ± 15 -nm band pass interference filter. The images presented for each wavelength were averaged over four frames and form part of a time course lasting 20 min, sampled at approximately 1–2-min intervals. The ratio image (C) was calculated pixel by pixel as the 488-nm image divided by the 442-nm image. Regions where the signal intensity fell below 10% of the average for the 442-nm image were masked in the ratio image by resetting to zero. Bright values correspond to high pH. Scale bar = 10 μ m.

multimode UV and visible HeCd units. Despite this the results are similar to the values obtained from the argon/krypton mixed-gas laser over a similar spectral range. Variations in focus at different wavelengths arise from axial chromatic aberration contributions from several optical components in the light path and vary with each objective lens. These focus differences between wavelengths will affect the confocal z -response most markedly in fluorescence. Large focus differences between excitation and emission wavelengths will result in misalignment of the illumination and fluorescence by as much as half the equivalent reflection plane response width. This could result in a 50% signal loss and halving of the practical z -resolution. The extent of this misalignment in z may affect image registration and optical sectioning with high-resolution dual labelling or ratio imaging studies.

Sample penetration and wavelength

In botanical specimens, the scattering properties of overlying structures are likely to have a significant influence on light penetration as the light path traverses a succession of heterogeneous highly refractive layers including the cuticle, cell wall, cytoplasm and vacuole. Our brief examination of tissue penetration suggests that wavelength-dependent scattering has several consequences. Near the surface, higher resolution and contrast results with lower wavelengths, whilst the red laser is better for probing deep into tissues. In multiple labelling studies, intensity differences from wavelength-dependent scattering will distort quantitative measurements.

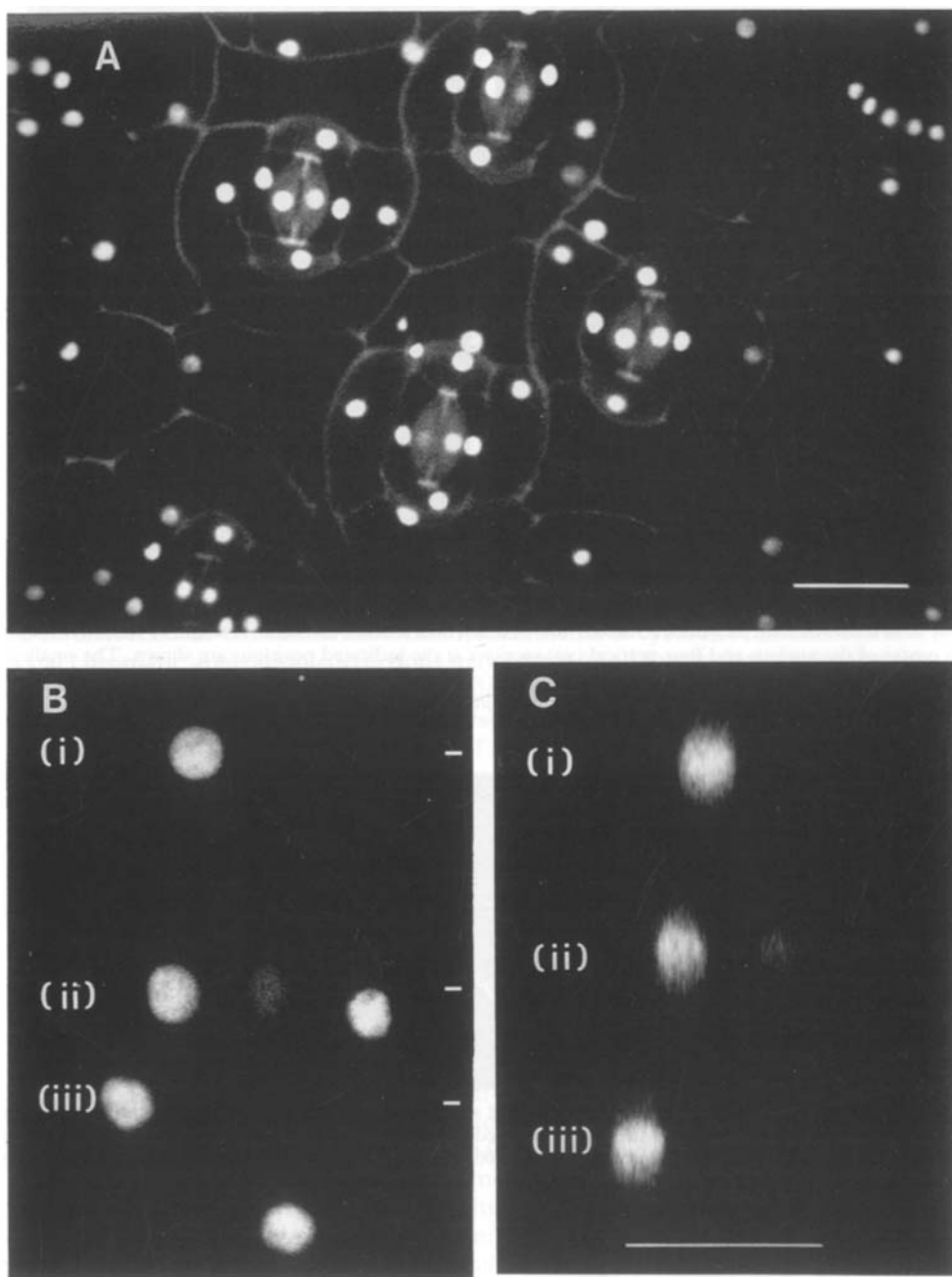


Fig. 6. Confocal imaging of DAPI-stained nuclei using excitation at 325 nm. (A) Single optical section of an epidermal peel from *Commelina communis* using a Nikon fluor $\times 100.5$ -NA lens: 325-nm excitation, 400–520-nm emission. Brightly stained nuclei are visible. The photomultiplier gain was set to detect the weak autofluorescence of the cell wall. Bright fluorescence from DAPI-stained nuclei saturated the dynamic range of the framestore under these conditions. Scale bar = 50 μm . (B) Maximum projection of twenty-eight optical sections collected at 1- μm intervals with a Nikon fluor $\times 40.0.85$ -NA lens. (C) Corresponding vertical (xz) sections taken from (B) along the transects indicated. Scale bar = 25 μm .

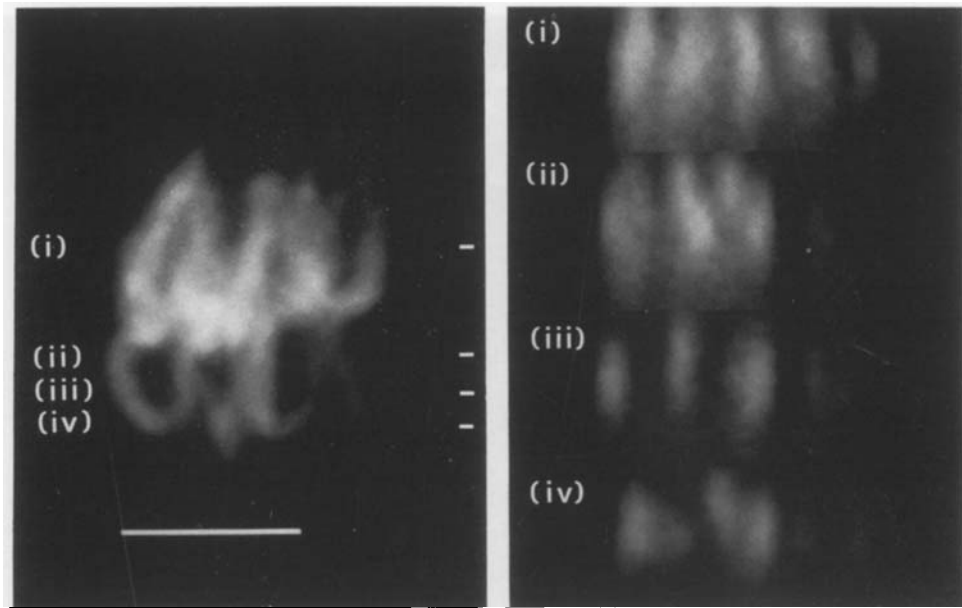


Fig. 7. Optical sections of a metaphase nucleus from a root tip cell of *Allium* stained with DAPI using a Nikon fluor $\times 40$ 0.85-NA lens: 325-nm excitation, 400–520-nm fluorescence emission. A single xy section through the centre of the nucleus and four vertical (xz) sections at the indicated positions are shown. The smallest chromosomes are approximately $1.5\ \mu\text{m}$ thick and the vertical sections indicate a z -axis resolution (width at half height) of approximately $3.5\ \mu\text{m}$. Scale bar = $20\ \mu\text{m}$.

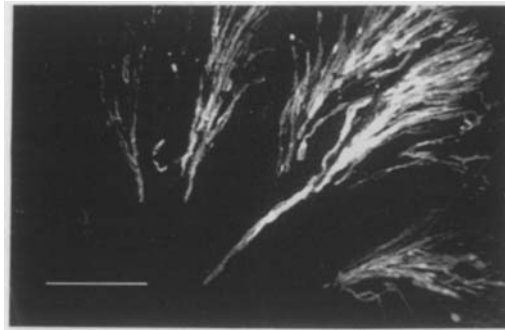


Fig. 8. Single optical section of an intact, four-lobed stigma from *Cordia alliodora*. Growth of compatible pollen tubes within the stigmatic tissues was visualized after staining with Aniline Blue using a Nikon fluor $\times 10$ 0.5-NA lens: 325-nm fluorescence excitation, 400–520-nm emission. Average of sixteen frames. Scale bar = $250\ \mu\text{m}$.

Confocal ratio imaging

Ratio imaging has been adopted as the method of choice in situations where quantification of fluorescent signals is critical. The main applications so far have centred on measurement of intracellular ion concentrations, but ratioing will find increasing use in a number of other imaging modes. These may include the ratioing of GC- versus AT-rich regions of heterochromatin or RGB reflection ratioing for colour analysis of images from wavelength-dependent absorption and scattering (Cogswell & Sheppard, 1990). Implementation of ratio measurements on confocal systems requires rigorous attention to chromatic problems. Correction of axial chromatic aberration will

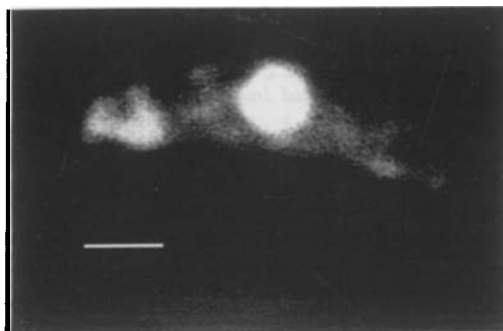


Fig. 9. Single optical section of guard cell from *Commelina communis* after micro-injection of the dual-emission calcium indicator dye, Indo-1. Average of twenty-one frames collected with a Nikon fluor $\times 10$ 0.5-NA lens: 325-nm excitation, 400–520-nm emission. Scale bar = 10 μm .

ensure correct registration of images in the z -axis. This will be most critical with particular wavelength combinations when undertaking high-resolution optical sectioning with the confocal aperture closed. Alteration of the ratio with depth and/or overlying structures is inevitable due to the different transparency of the tissue at different wavelengths, requiring careful sample preparation and limiting the accuracy of quantification with heterogeneous living specimens.

The high excitation efficiency of BCECF and Fura-Red by the HeCd and argon-ion lasers enables dual-excitation confocal measurements of cytosolic free calcium and pH. Axial chromatic aberration corrections may be required for critical confocal measurements. This requires access to each wavelength component separately, which can be readily achieved with a multiple-laser system. A single-emission wavelength allows very broad band detection (at some loss of resolution due to chromatic problems) and consequently good signal-to-noise ratios. However, sequential excitation at two wavelengths reduces temporal resolution. Single-excitation dyes such as Indo-1 give better temporal resolution, but require separation and correction of two emission wavelengths. Selection of narrow emission bands increases the sensitivity of the ratio to changes in ion concentration at the expense of the signal-to-noise ratio.

UV-excited confocal fluorescence

UV confocal imaging with most microscope objectives demands axial chromatic correction. A practical solution is to introduce pre-focusing of the excitation beam, in combination with the best flat-field (plan) objectives and some reduction in the field of view. Our first confocal images of Indo-1 reveal some information about the subcellular distribution of the dye and encourage dual-emission ratioing for quantitative calcium measurements. Optical transmission efficiency at 325 nm currently prevents us from imaging with objectives of NA higher than 0.85. Although considerable detail is visible in the optical sections of DAPI-stained metaphase chromosomes of *Allium* (Fig. 7), they are not yet comparable to our results with Chromomycin A3 (Fig. 4). We are currently examining high-NA UV-transmitting objectives to address this problem.

ACKNOWLEDGMENTS

M.D.F. would like to thank the Nuffield Foundation, Royal Society and AFRC for financial support. N.S.W. thanks the SERC for support. We also acknowledge Bio-Rad Microscience Ltd, Spindler and Hoyer Ltd and Lambda Photometrics Ltd for the loan of equipment and technical information. Some of the equipment for this work was obtained by grants from the SERC and CRC to D. M. Shotton, Zoology Department, Oxford. We are grateful to D. Boshier and A. Kenton for supplying the pollen material.

REFERENCES

- Boyde, A. (1985) The tandem scanning reflected light microscope. *Proc. Roy. Microsc. Soc.* **20**, 130–139.
- Brakenhoff, G.J., Binnerts, J.S. & Woldringh, C.L. (1980) Developments in high resolution confocal scanning light microscopy (CSLM). *Scanned Image Microscopy* (ed. by E. A. Ash), pp. 183–200. Academic Press, London.
- Brakenhoff, G.J., Blom, P. & Barends, P. (1979) Confocal scanning light microscopy with high aperture immersion lenses. *J. Microsc.* **117**, 219–232.
- Cogswell, C.J. & Sheppard, C.J.R. (1990) Confocal brightfield imaging techniques using an on-axis scanning optical microscope. *Confocal Microscopy* (ed. by T. Wilson), pp. 213–243. Academic Press, London.
- Fricker, M.D. & White, N.S. (1990) Volume measurement of guard cell vacuoles during stomatal movements using confocal microscopy. *Trans. Roy. Microsc. Soc.*, Vol. 1 (ed. by H. Y. Elder), pp. 345–348. Adam Hilger, Bristol.
- Gilroy, S.G., Fricker, M.D., Read, N.R. & Trewavas, A.J. (1991) Role of calcium in signal transduction of *Commelina* guard cells. *The Plant Cell*, **3**, 333–334.
- Kuba, K., Hua, S.Y. & Nohmi, M. (1991) Spatial and dynamic changes in intracellular Ca^{2+} measured by confocal laser-scanning microscopy in bullfrog sympathetic ganglion cells. *Neurosci. Res.* **10**, 245–256.
- Lloyd, C.W. (1987) The plant cytoskeleton: the impact of fluorescence microscopy. *Ann. Rev. Plant Physiol.* **38**, 119–139.
- Minsky, M. (1961) *Microscopy apparatus*. US Patent No. 3013467, filed 7 November 1957, granted 19 December 1961.
- Montag, M., KuKulies, J., Jorgens, R., Gundlach, H. & Trendelenburg, M.F. (1991) Working with the confocal scanning UV-laser microscope: specific DNA localisation at high sensitivity and multiple parameter fluorescence. *J. Microsc.* **163**, 201–210.
- Petran, M. & Hadravsky, M. (1967) *Method and arrangement for improving the resolving power and contrast*. US Patent No. 3517980, filed 4 December 1967, granted 30 June 1970.
- Read, N.D., Allan, W.T.G., Knight, H., Knight, M.R., Malho, R., Russell, A., Shacklock, P.S. & Trewavas, A.J. (1992) Imaging and measurement of cytosolic free calcium in plant and fungal cells. *J. Microsc.* **166**, 57–86.
- Robards, A.W. (1985) *Botanical Microscopy*. Oxford University Press, Oxford.
- Shotton, D.M. (1989) Review: confocal scanning optical microscopy and its applications for biological specimens. *J. Cell. Sci.* **94**, 175–206.
- White, N.S., Bennett, S.T., Kenton, A.Y., Callimassia, M.A. & Fricker, M.D. (1991) Characterising plant chromosomes and their 3D organisation using CLSM. *Scanning*, **13**, Supplement I, 1–128.